Modelling the forced response of a stiffened structure

James A. FORREST[1]

[1] Defence Science & Technology Organisation, 506 Lorimer St, Fishermans Bend VIC 3207, Australia

ABSTRACT

Different analytical approaches can be used to model the forced response of the beam-stiffened plates or shells that are commonly found in many practical structures from ships to aircraft. A popular method is to smear the mass and stiffness properties of the beam stiffeners to give an orthotropic plate or shell. This is simpler than modelling discrete stiffeners. This paper considers the example problem of a cylindrical shell with ring stiffeners. Previous work using periodic structure theory has shown that the calculated wave propagation behaviour in this cylinder using a smeared shell model is different from that with the stiffeners modelled discretely. The current work calculates the forced response of the cylinder using both models and compares the results to determine the range of applicability of the smeared shell approach.

Keywords: Vibration, Structures, Transmission, Analytical Models
I-INCE Classification of Subjects Number(s): 43.2, 75.9

1. INTRODUCTION

Plates and shells are basic structural building blocks and their dynamics have been of interest since the earliest investigations in mechanics. Stiffeners in the form of beams of various cross-sections are used in many plate and shell structures to increase stiffness and strength with a minimal increase in weight. Earlier work on stiffened plates and stiffened cylindrical shells is described by Leissa (1, 2). These approaches treat the stiffened structure as an equivalent orthotropic one, i.e. the stiffeners' mass and stiffness is effectively smeared over the continuous plate or shell. As noted by Leissa (2) and compared by Ruotolo (3), there are a number of thin-shell theories, which differ in the terms included to account for shell bending.

The advantage of smearing the stiffener properties is that it makes the solution of the plate or shell dynamics only a little more complicated than the uniform isotropic case. Gan *et al.* (4) apply the smeared approach in a wave propagation method to solve the natural frequencies of a ring-stiffened cylindrical shell. Luan *et al.* (5) propose improvements to the smeared approximation for cross-stiffened rectangular plates. Beyond simple smearing, Junger and Feit (6) consider reaction forces on a plate due to just the translational and rotary inertia of regularly spaced stiffeners.

Large structures with evenly spaced stiffeners can be analysed as infinite periodic structures. Structural periodicity results in pass and stop bands of vibration transmission which are not accounted for in smeared-stiffener analysis. Mace (7) considers infinite fluid-loaded stiffened plates excited by line and point forces, giving general expressions for the stiffener reaction forces and moments and specific values for beam-like stiffeners. Langley (8) applies the periodic method to a chain of plates joined end to end, each with two sides simply supported and a stiffener at the joins. He also discusses the use of a dynamic stiffness matrix for a single plate unit in assembling a structure with varied stiffener spacing from a finite number of plate units. Hodges *et al.* (9) model an infinitely long ring-stiffened cylindrical shell using Fourier decomposition and space-harmonic analysis, with the cross-section of the symmetric stiffeners allowed to distort. Mead and Bardell (10) investigate wave propagation in a cylinder with axial stiffeners (stringers), and in a cylinder with circumferential (ring) stiffeners in (11). They allow for stiffeners of arbitrary cross-section. The approach assumes periodicity in the circumferential or axial direction respectively, and seeks propagation constants that are related to the wave types in the cylinder. They note that either axial or circumferential stiffeners can be considered with this method, but not both together. Lee and Kim (12) apply a similar method for sound transmission through a ring-stiffened aircraft fuselage, but treat each stiffener as a lumped mass, translational spring and rotational spring. Efimtsov and Lazarev (13) demonstrate a solution for periodically stiffened

[1] james.forrest@dsto.defence.gov.au

plates and shells using space-harmonic expansions which is more amenable at high frequencies than the propagation constant method. Solaroli *et al.* (14) analyse periodically stiffened shells numerically using the finite-element method.

A cylindrical shell with ring stiffeners will be considered in this paper. Such shells are of practical interest in many applications. A cylindrical shell is equivalent to a plate rolled up, but the introduction of the curvature couples all three displacement components together. This makes its dynamics more interesting than a flat plate, where the bending vibration is decoupled from the two in-plane components. Periodic structure theory was applied in Forrest (15) to compare the wave propagation in a plain cylindrical shell, the shell with smeared stiffener properties, and the shell with discrete stiffeners. The propagation parameters were different in each case. The techniques of that paper will be refactored in this one to consider the forced vibration of a cylinder with ring stiffeners, modelled using both a smeared shell approach and a discrete stiffener approach.

2. MODELLING

The equations of motion for a thin cylindrical shell including the option of smeared ring stiffeners will be presented. These can then be used to calculate the wavenumbers for free vibration propagation in a length of cylinder. Consideration of the general force boundary conditions along with the general displacement functions allows the calculation of the dynamic stiffness matrix for the length of cylinder either from the smeared shell approach or plain shell with discrete stiffener approach. A number of dynamic stiffness matrices can be assembled to model a finite cylinder with several ring stiffeners. This allows the calculation of the forced response of the stiffened cylinder using either model.

2.1 Equations of Motion

Figure 1 shows a thin cylindrical shell of radius R, thickness h and length L. Also shown is the coordinate system x (longitudinal), y (tangential) and z (radial) centred on an element of the shell surface which is at angular position θ.

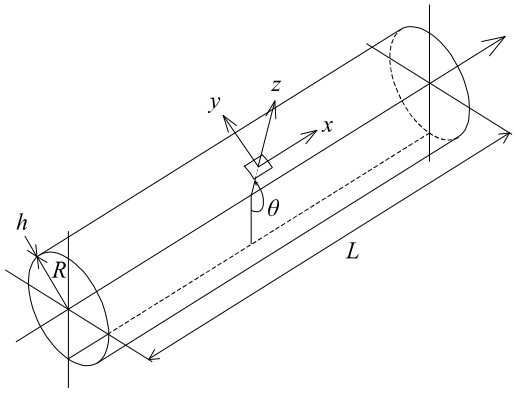

Figure 1 – A cylindrical shell of radius R, thickness h and length L showing the coordinate system used.

A thin cylindrical shell with ring stiffeners will be considered here. Leissa (2) gives results for a number of orthotropic shell formulations. When these are applied to shells with individual stiffeners, the stiffener properties are effectively smeared over the whole shell. If the approach of Mikulas and McElman, quoted in Leissa (2), is simplified to consider only ring stiffeners and ignore longitudinal stringers, and inertia terms and general distributed forces are also added in, the equations of motion presented in Forrest (15) are the result. They are the Donnell-Mushtari shell equations with extra terms for the stiffeners. These can be modified to use the Love-Timoshenko shell equations given in Mead and Bardell (10), to better match the force expressions in Mead and Bardell (11), which are developed from the same shell equations. Compared to the Donnell-Mushtari equations, the Love-Timoshenko and other alternative thin shell equations include extra terms for shell bending, which can better model the bending effects in shells with higher thickness-to-radius ratios. The three equations of motion for equilibrium along each coordinate are

$$R^2 u_{xx} + \frac{(1-\nu)}{2} u_{\theta\theta} - \frac{\rho(1-\nu^2)R^2}{E} \ddot{u} + \frac{(1+\nu)R}{2} v_{x\theta} + \nu R w_x + \frac{(1-\nu^2)R^2}{Eh} q_1 = 0 \qquad (1)$$

$$\frac{(1+\nu)R}{2}u_{x\theta}+\frac{(1-\nu)R^2}{2}(1+4\beta)v_{xx}+[1+\beta+s_A]v_{\theta\theta}-\frac{\rho(1-\nu^2)R^2}{E}\ddot{v}+[1+s_A]w_\theta$$
$$-(2-\nu)R^2\beta w_{xx\theta}-[\beta+s_z]w_{\theta\theta\theta}+\frac{(1-\nu^2)R^2}{Eh}q_2=0 \quad (2)$$

$$\nu R u_x+[1+s_A]v_\theta-(2-\nu)R^2\beta v_{xx\theta}-[\beta+s_z]v_{\theta\theta\theta}+[1+s_A]w-2s_z w_{\theta\theta}+R^4\beta w_{xxxx}$$
$$+2R^2\beta\big[1+s_J\big]w_{xx\theta\theta}+\beta[1+s_I]w_{\theta\theta\theta\theta}+\frac{\rho(1-\nu^2)R^2}{E}\ddot{w}-\frac{(1-\nu^2)R^2}{Eh}q_3=0 \quad (3)$$

where u, v and w are the displacements and q_1, q_2 and q_3 are the external forces per unit area in the x, y and z directions respectively. These forces are set to zero to calculate natural frequencies or free waves in the shell. They can also be expressed as Dirac delta functions to represent point forces in the middle of the shell between boundaries, but this will not be used in this paper. $\beta \equiv h^2/12R^2$ is the thickness ratio. The subscripts x and θ on u, v and w denote differentiation with respect to those variables, while dot denotes differentiation with respect to time. The shell and the ring stiffeners are assumed to be of the same material with a Young's modulus E and Poisson's ratio ν.

The ring stiffeners placed along the cylinder give rise to the shell stiffener parameters

$$s_A \equiv \frac{A(1-\nu^2)}{ah} \qquad s_z \equiv \frac{\bar{z}A(1-\nu^2)}{ahR} \qquad s_J \equiv \frac{3J(1-\nu)}{ah^3} \qquad s_I \equiv \frac{12(I_{xx}+\bar{z}^2A)(1-\nu^2)}{ah^3} \quad (4)$$

where a is the axial spacing of the stiffeners, and the stiffener cross-section has area A, second moment of area I_{xx}, torsion constant J and its centroid is a distance of $\overline{z}$ from the shell middle surface. Using the parameters in Equations (4) smears the stiffener properties across the shell. Setting them all to zero, i.e. $s_A = s_z = s_J = s_I = 0$, gives the equations of motion for a plain (uniform isotropic) shell.

For a plain shell, ρ is the density of the shell material. When the stiffeners are included, ρ is M/h where M is the average smeared out mass per unit area of the stiffened shell, i.e. incorporating the mass of the stiffeners. If the stiffener's cross-sectional dimensions are small compared to the radius R, then the effective density is

$$\rho = (1 + A/ah)\rho_{material} \quad (5)$$

For the smeared model, it can be seen from Equation (1) that the only effect on the axial equilibrium equation of adding ring stiffeners is this added mass.

2.2 Calculation of wavenumbers and displacements

To solve for free waves in the shell, harmonic solutions of the form

$$u = Ae^{ikx}\cos n\theta\, e^{-i\omega t}$$
$$v = Be^{ikx}\sin n\theta\, e^{-i\omega t} \quad (6)$$
$$w = Ce^{ikx}\cos n\theta\, e^{-i\omega t}$$

are substituted into Equations (1) to (3), where each displacement function is described by the axial wavenumber k which is to be solved as a function of circumferential mode number n and angular frequency ω. The complex exponential sign convention used here means that positive real values of k correspond to waves propagating in the positive x-direction, while positive imaginary values correspond to evanescent waves decaying in the same direction. With this convention, damping can be included in the model by replacing E by a complex modulus $E(1-i\eta)$ where η is the loss factor of the material.

The substitution of solutions (6) into the equations of motion leads to three simultaneous equations that can be written in the matrix form

$$\begin{bmatrix} b_{11} & b_{12} & b_{13} \\ b_{21} & b_{22} & b_{23} \\ b_{31} & b_{32} & b_{33} \end{bmatrix}\begin{bmatrix} A \\ B \\ C \end{bmatrix} = \begin{bmatrix} 0 \\ 0 \\ 0 \end{bmatrix} \quad (7)$$

where the matrix coefficients are functions of the previously defined parameters given by

$$
\begin{aligned}
b_{11} &= -R^2k^2 - (1-\nu)n^2/2 + \Omega^2 \\
b_{12} &= i\,(1+\nu)Rnk/2 \\
b_{13} &= i\nu Rk \\
b_{21} &= -i\,(1+\nu)Rnk/2 \\
b_{22} &= -\,(1-\nu)R^2(1+\beta)k^2/2 - [1+\beta+s_A]n^2 + \Omega^2 \\
b_{23} &= -[1+s_A]n - (2-\nu)R^2\beta nk^2 - [\beta+s_z]n^3 \\
b_{31} &= i\nu Rk \\
b_{32} &= [1+s_A]n + (2-\nu)R^2\beta nk^2 + [\beta+s_z]n^3 \\
b_{33} &= [1+s_A] + 2s_zn^2 + R^4\beta k^4 + 2R^2\beta\big[1+s_J\big]n^2k^2 + \beta[1+s_I]n^4 - \Omega^2
\end{aligned}
\tag{8}
$$

with the additional non-dimensional frequency parameter $\Omega^2 \equiv \rho(1-\nu^2)R^2\omega^2/E$, which is the squared ratio of the frequency to the shell ring frequency. The ring frequency is that of the "breathing" mode of the whole shell, where the wavelength of longitudinal waves is equal to the shell circumference.

Equation (7) has a non-trivial solution when the determinant of the matrix is zero. The determinant can be expanded out explicitly in terms of the coefficients b_{ij} to give a quartic polynomial in k^2. This can be solved numerically to eventually give eight values of k for a given frequency ω and mode number n. Substituting each of these values of k back into the matrix equation in turn allows the calculation of the corresponding values of A, B and C. Since the determinant is zero, the rows of the matrix are no longer linearly independent and these coefficients can only be found as relative values, such as the ratios A/C and B/C. These ratios can be calculated from any two rows of the matrix in Equation (7). One solution is

$$
\frac{A_{sn}}{C_{sn}} \equiv \varphi_{sn} = \frac{-b_{13}b_{22} + b_{12}b_{23}}{b_{11}b_{22} - b_{12}b_{21}} \qquad \frac{B_{sn}}{C_{sn}} \equiv \psi_{sn} = \frac{b_{13}b_{21} - b_{11}b_{23}}{b_{11}b_{22} - b_{12}b_{21}} \tag{9}
$$

where the subscript s refers to the particular wavenumber (1 to 8). The ratios A_{sn}/C_{sn} and B_{sn}/C_{sn} can be considered to determine the relative amounts of motion in each direction associated with each wavenumber. For example, if A_{sn}/C_{sn} is large and B_{sn}/C_{sn} is small, then the motion is predominantly axial. If both ratios are less than unity, then the motion is predominantly radial, and so on.

Thus the coefficients A and B in solutions (6) can be written in terms of C. The total displacements are the sum of the contributions from each wavenumber relevant to the problem at hand. They can be written as

$$
\begin{aligned}
u &= \sum_{n=0}^{\infty}\sum_{s=1}^{8} \varphi_{sn}C_{sn}e^{ik_{sn}x}\cos n\theta\; e^{-i\omega t} \\
v &= \sum_{n=0}^{\infty}\sum_{s=1}^{8} \psi_{sn}C_{sn}e^{ik_{sn}x}\sin n\theta\; e^{-i\omega t} \\
w &= \sum_{n=0}^{\infty}\sum_{s=1}^{8} C_{sn}e^{ik_{sn}x}\cos n\theta\; e^{-i\omega t}
\end{aligned}
\tag{10}
$$

showing the sum of terms due to the eight roots for k_{sn} over the range of circumferential mode numbers n. Each root has its negative counterpart, so the two represent a pair of waves, one travelling in the positive x-direction, the other in the negative x-direction. While an infinite number of circumferential modes have been included, in practice only as many as needed to reach convergence have to be used.

2.3 Forces acting on the ends of a cylindrical section

The displacements in Equations (10) are functions of the unknown coefficients C_{sn}. These can be solved from a knowledge of the boundary conditions acting on a length of cylinder. This length can be taken as the section of cylindrical shell between ring stiffeners, or for the smeared shell model, the total length of the cylinder. To construct a dynamic stiffness matrix for this length, generalised end forces are required. The force convention that will be used is that forces are positive in the direction that their corresponding displacements are positive. This gives dynamic stiffness matrices that are suitable for assembly in the same way as stiffness matrices are assembled in the finite-element method. The end forces and moments per unit length acting on a cylindrical unit of length a are shown in Figure 2. They are shown across an isometric view and a side view. The forces act around the whole circumference of the ends, but for clarity are only shown at part of the circumference on the diagram at the left and at the top of the diagram on the right.

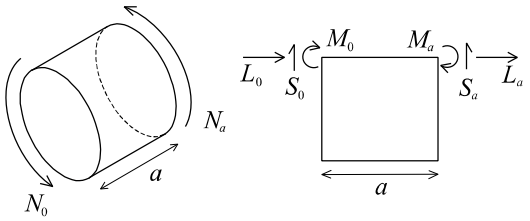

Figure 2 – The line forces and moments acting on the ends of cylindrical unit, isometric and side views.

Expressions for the end forces are given by Mead and Bardell (11). These allow for stiffeners of arbitrary open, not necessarily symmetric, cross-section. If a stiffener is of rectangular section of width b and depth d, which is a symmetric and relatively slender section, the Wagner torsion-bending constant Γ can be taken as zero, as can the product moment of area I_{xz}. Taking account of the required sign convention, the end force expressions can then be simplified to the following formulae.

$$\begin{aligned} RM_{0,a} = {} & \mp\frac{Eh^3R}{12(1-\nu^2)}\left\{w_{xx}+\frac{\nu}{R^2}(w_{\theta\theta}-v_\theta)\right\} \\ & \mp\frac{1}{2}\left[-\frac{EI_{zz}}{R}\left(w_x-\frac{u_{\theta\theta}}{R}\right)-\frac{EAb}{2R}(w+v_\theta)+\frac{GJ}{R}\left(w_{x\theta\theta}-\frac{u_{\theta\theta}}{R}\right)\right. \\ & \left. -R\rho\left(I_{xx}\ddot{w}_x+I_{zz}\ddot{w}_x-\frac{Ad}{2}\ddot{u}+\frac{Ab}{2}\ddot{w}\right)\right] \end{aligned} \tag{11}$$

$$\begin{aligned} RS_{0,a} = {} & \pm\frac{Eh^3R}{12(1-\nu^2)}\left\{w_{xxx}+\frac{(2-\nu)}{R^2}(w_{x\theta\theta}-v_{x\theta})\right\} \\ & \mp\frac{1}{2}\left[\frac{EA}{R}\left(w+v_\theta+\frac{b}{2}w_x+\frac{d}{2R}v_\theta-\frac{d}{2R}w_{\theta\theta}-\frac{b}{2R}u_{\theta\theta}\right)+\frac{EI_{xx}}{R^3}(w_{\theta\theta\theta\theta}-v_{\theta\theta\theta})\right. \\ & \left. -\frac{EAd}{2R^2}(w_{\theta\theta}+v_{\theta\theta\theta})-R\rho\left(\frac{I_{xx}}{R^2}\ddot{w}_{\theta\theta}-\frac{I_{xx}}{R^2}\ddot{v}_\theta-\frac{Ad}{2R}\ddot{v}_\theta\right)+R\rho A\left(\ddot{w}+\frac{b}{2}\ddot{w}_x\right)\right] \end{aligned} \tag{12}$$

$$\begin{aligned} RN_{0,a} = {} & \mp\frac{EhR}{2(1-\nu^2)}\left\{(1-\nu)\left(v_x+\frac{u_\theta}{R}\right)-4\beta(1-\nu)(w_{x\theta}-v_x)\right\} \\ & \mp\frac{1}{2}\left[-\frac{EA}{R}\left(v_{\theta\theta}+w_\theta+\frac{d}{2R}w_\theta+\frac{b}{2}w_{x\theta}+\frac{d}{R}v_{\theta\theta}-\frac{d}{2R}w_{\theta\theta\theta}-\frac{b}{2R}v_{\theta\theta}\right)\right. \\ & \left. +\frac{EI_{xx}}{R^3}(w_{\theta\theta\theta}-v_{\theta\theta})+R\rho\left(A\ddot{u}+\frac{Ad}{R}\ddot{v}-\frac{Ad}{2R}\ddot{w}_\theta-\frac{Ab}{2R}\ddot{u}_\theta+\frac{I_{xx}}{R^2}\ddot{v}-\frac{I_{xx}}{R^2}\ddot{w}_\theta\right)\right] \end{aligned} \tag{13}$$

$$\begin{aligned} RL_{0,a} = {} & \mp\frac{EhR}{(1-\nu^2)}\left\{u_x+\frac{\nu}{R}(w+v_\theta)\right\} \\ & \mp\frac{1}{2}\left[\frac{EI_{zz}}{R}\left(\frac{u_{\theta\theta\theta}}{R^2}-\frac{w_{x\theta\theta}}{R}\right)-\frac{Eab}{2R^2}(w_{\theta\theta}+v_{\theta\theta\theta})-\frac{GJ}{R}\left(\frac{u_{\theta\theta}}{R^2}-\frac{w_{x\theta\theta}}{R}\right)\right. \\ & \left. +R\rho A\left(\ddot{u}-\frac{d}{2}\ddot{w}_x\right)-R\rho\left(\frac{I_{zz}}{R^2}\ddot{u}_{\theta\theta}-\frac{Ab}{2R}\ddot{v}_\theta\right)\right] \end{aligned} \tag{14}$$

These are based on Love-Timoshenko shell theory, as are the equations of motion (1) to (3). Where there are plus-minus signs, the top sign corresponds to the expression for the end at $x = 0$, while the bottom sign is for the end at $x = a$. The first term in each expression, grouped with curly brackets, represents the contribution of shell deformation to the forces. The remaining terms represent the contribution of beam stiffener deformation to the forces. The factor of one-half outside this second group of terms in each force expression is because only half a stiffener is considered at each end of the cylinder unit. When cylinder units are assembled, the two halves give a whole stiffener at the join.

To model a cylindrical shell with the smeared stiffener approach, only the shell contribution terms in the forces are used, with the stiffener terms included in the displacement solutions. To model discrete stiffeners, the full force expressions above are used, with the displacement solutions derived from the equations for a plain shell, i.e. without added stiffener parameters.

2.4 Calculation of the dynamic stiffness matrix

The dynamic stiffness matrix relates the forces at the ends $x = 0$ and $x = a$ of a cylinder unit to the displacements at the ends of the unit. A displacement vector $\mathbf{u}$ and force vector $\mathbf{f}$ can be made up of these forces and displacements as

$$\begin{aligned} \mathbf{u} &= [u_0 \quad v_0 \quad w_0 \quad w_0' \quad u_a \quad v_a \quad w_a \quad w_a']^T = \sum_{n=0}^{\infty} \mathbf{U}_n \begin{matrix}\cos\\ \sin\end{matrix} (n\theta)\, e^{-i\omega t} \\ \mathbf{f} &= [L_0 \quad N_0 \quad S_0 \quad M_0 \quad L_a \quad N_a \quad S_a \quad M_a]^T = \sum_{n=0}^{\infty} \mathbf{F}_n \begin{matrix}\cos\\ \sin\end{matrix} (n\theta)\, e^{-i\omega t} \end{aligned} \tag{15}$$

where "sin" is used for the tangential displacement $v_{0,a}$ and tangential force $N_{0,a}$ and "cos" is used for all other forces and displacements. The elements of these vectors are the forces and displacements developed earlier, calculated at the ends as denoted by their subscript. Dash indicates derivative with respect to x, so that the $w_{0,a}'$ elements are rotations.

The elements of the modal harmonic displacement and force vectors $\mathbf{U}_n$ and $\mathbf{F}_n$ can be calculated from the displacement equations (10) and the force equations (11) to (14), as functions of the coefficients C_{sn}. They can be written in matrix form as

$$\mathbf{U}_n = [\mathbf{P}_n]\mathbf{C}_{sn} \qquad \mathbf{F}_n = [\mathbf{Q}_n]\mathbf{C}_{sn} \tag{16}$$

where $\mathbf{C}_{sn}$ is the vector of the eight unknown coefficients. Matrices $[\mathbf{P}_n]$ and $[\mathbf{Q}_n]$ are functions of ω, n and the wavenumbers k_{sn}, as well as the ratio quantities φ_{sn} and ψ_{sn}. The rows relating to forces or displacements at $x = a$ also contain exponential terms of the form $e^{ik_{sn}a}$. The two equations (16) can be used to eliminate $\mathbf{C}_{sn}$, giving

$$\mathbf{F}_n = [\mathbf{Q}][\mathbf{P}]^{-1}\mathbf{U}_n = [\mathbf{K}_n]\mathbf{U}_n \tag{17}$$

where $[\mathbf{K}_n]$ is the dynamic stiffness matrix.

A number of these dynamic stiffness matrices can be assembled as in the finite-element method to model several cylindrical units joined end-to-end. This process gives a larger dynamic stiffness matrix which is heavily banded about the diagonal. Of course, each component matrix describes a bigger part of the structure than a finite element does, so the representation is still relatively compact. For example, if the 8 by 8 matrix $[\mathbf{K}_n]$ is partitioned into 4 by 4 blocks as

$$[\mathbf{K}_n] = \begin{bmatrix} \mathbf{K}_{11} & \mathbf{K}_{12} \\ \mathbf{K}_{21} & \mathbf{K}_{22} \end{bmatrix} \tag{18}$$

then the assembled matrix $[\mathbf{K}_n]_5$ to model the larger structure of 5 identical units joined together takes the form

$$[\mathbf{K}_n]_5 = \begin{bmatrix} \mathbf{K}_{11} & \mathbf{K}_{12} & 0 & 0 & 0 & 0 \\ \mathbf{K}_{21} & \mathbf{K}_{22}+\mathbf{K}_{11} & \mathbf{K}_{12} & 0 & 0 & 0 \\ 0 & \mathbf{K}_{21} & \mathbf{K}_{22}+\mathbf{K}_{11} & \mathbf{K}_{12} & 0 & 0 \\ 0 & 0 & \mathbf{K}_{21} & \mathbf{K}_{22}+\mathbf{K}_{11} & \mathbf{K}_{12} & 0 \\ 0 & 0 & 0 & \mathbf{K}_{21} & \mathbf{K}_{22}+\mathbf{K}_{11} & \mathbf{K}_{12} \\ 0 & 0 & 0 & 0 & \mathbf{K}_{21} & \mathbf{K}_{22} \end{bmatrix} \tag{19}$$

where the zeros represent 4 by 4 blocks of zeros. This can be generalised to the dynamic stiffness matrix $[\mathbf{K}_n]_N$ to represent N units joined up. This matrix has $N + 1$ blocks along the diagonal band, or in other words is $4(N + 1)$ by $4(N + 1)$ elements in size. It can be used in place of $[\mathbf{K}_n]$ in Equation (17), with the vectors $\mathbf{F}_n$ and $\mathbf{U}_n$ also replaced by larger vectors representing all the forces and displacements at the unit boundaries, including the free ends of the assembled structure.

A point force at the end can be represented as a Dirac delta function of the angular position θ. For a longitudinal or radial force acting at $\theta = 0$, this can be written as a Fourier cosine series as follows.

$$F_0 = \frac{\delta(\theta)}{a} = \frac{1}{2\pi a} + \sum_{n=1}^{\infty} \frac{1}{\pi a} \cos n\theta \tag{20}$$

For the response of a single cylindrical unit, the appropriate force component in the vector $\mathbf{F}_n$ in Equation (17) is set to $1/2\pi a$ for $n = 0$ or $1/\pi a$ for values of $n \geq 1$. This allows the calculation of the corresponding $\mathbf{U}_n$, which can then be summed according to the first of Equations (15) to give the total displacements. A similar process is followed for the response of several cylindrical units joined together, using instead the larger dynamic stiffness matrix assembled from several of those for a single unit.

3. RESULTS AND DISCUSSION

The cylindrical shell considered here is based on the plain (unstiffened) steel shell for which experimentally determined modes and natural frequencies are compared to theoretical ones in Forrest (16), and sound radiation and active control are analysed in Forrest (17). The notional stiffener parameters are similar to Forrest (15), but with a depth of 12 mm instead of 30 mm to keep the depth to radius ratio small. The shell and ring stiffener properties used to generate the results are given in Table 1.

Other parameter values are derived from these, such as $G = E/2(1+\nu)$, $I_{xx} = bd^3/12$ and $I_{zz} = b^3 d/12$. Young and Budynas (18) give formulae for the torsion constant J, which they denote K, for various cross-sections. For a rectangular cross-section, the torsion constant is given within 4% accuracy by

$$J = b^3 d \left[\frac{1}{3} - 0 \cdot 21 \frac{b}{d}\left(1 - \frac{b^4}{12d^4}\right)\right] \tag{21}$$

for the notation used here, with $d > b$. The loss factor η is applied to the Young's modulus E to give a complex modulus, as described earlier.

Table 1 – Properties of the cylindrical shell and ring stiffeners

Quantity	Symbol	Value
Shell radius	R	200 mm
Shell thickness	h	2 mm
Shell length	L	1.5 m
Stiffener spacing	a	100 mm
Stiffener width	b	4 mm
Stiffener depth	d	12 mm
Young's modulus	E	210 GPa
Loss factor	η	0.01
Poisson's ratio	ν	0.3
Density	ρ	7800 kg/m^3

3.1 Numerical Considerations

The software package Matlab was used to generate the results in the following section. However, this presented some numerical challenges, at least for the parameters of the example cylinder considered. Attempting to use numerical polynomials in Equation (7) and then calculate the determinant of the matrix to obtain the numerical polynomial in k^2 failed to give correct roots for k, and sometimes even only generated a cubic equation in k^2 rather than a quartic one. This was because the spread of numerical values of the polynomial coefficients was too great, leading to significant round-off error. Instead, the wxMaxima computer algebra system was used to expand the determinant of Equation (7) symbolically and hence give symbolic expressions for the coefficients of the quartic polynomial in k^2. These coefficients were then used in Matlab to calculate the roots of the characteristic equation numerically.

The matrices used to calculate the dynamic stiffness matrix in Equation (17) can be badly scaled because of the rows containing the exponential terms $e^{ik_{sn}a}$. When a particular root k_{sn} has a negative imaginary part, the corresponding exponential expressions can be very large numerically, as the overall exponent has a positive real part. The matrices still contain very small numerical values as well. This poor scaling leads to matrices that are numerically close to singular, and consequently to an inaccurate and badly scaled dynamic stiffness matrix. The scaling method described by Langley (8) was adapted to address this. The coefficients C_{sn} corresponding to the problem roots are replaced by scaled coefficients $C_{sn}e^{-ik_{sn}a}$ in both of Equations (16). With this substitution, the corresponding elements in $[\mathbf{P}_n]$ and $[\mathbf{Q}_n]$ are multiplied by $e^{-ik_{sn}a}$. This cancels the $e^{ik_{sn}a}$ terms in the problem matrix elements. This is all that is needed to accurately calculate the dynamic stiffness matrix from Equation (17) and then determine end forces or displacements. However, the scaling has to be eventually backed out if calculating displacements across a unit from Equations (10), as this makes use of the now scaled coefficient vectors $\mathbf{C}_{sn}$ that would be derived from Equations (16) with known

end states of force or displacement.

It was found that computations using assembled dynamic stiffness matrices of the type illustrated by Equation (19) could be sped up by using sparse matrix storage and sparse matrix computation methods. The time taken was about one third less for each effective inversion of $\mathbf{K}_n$ to calculate $\mathbf{U}_n$ from Equation (17), compared to using the fully dense version of the assembled matrix. While this is perhaps trivial for the calculations here, which take a minute or two to complete, it could be significant for matrices representing much larger assemblies of cylindrical units.

The summations for total displacements, such as in Equations (10) and (15), begin from $n = 0$. This is the axisymmetric case, i.e. $v = 0$, and renders the matrices in the previous development singular and unusable for calculation of displacements. A separate axisymmetric formulation would be needed to generate the $n = 0$ terms for u and w. Therefore only the terms for $n \geq 1$ were used in the summations to generate results. This may neglect some axisymmetric axial modes. However, for radial motion, the $n = 0$ terms become most important around and above the ring frequency, which is 4328 Hz for plain shell sections using the parameters in Table 1. The results in the next section are considered for frequencies well below this, and so are still a reasonable basis for comparing the two modelling approaches.

3.2 Forced response results

A shell with smeared stiffeners was modelled by single dynamic stiffness matrices calculated for each n using the full length L of 1.5 m. A shell with discrete stiffeners for comparison was modelled for each n by assembling $N = 15$ dynamic stiffness matrices, each representing a cylindrical unit of length a, the stiffener spacing of 0.1 m. The smeared stiffener shell model included the stiffener parameters (4) in the equations of motion (1) to (3) and hence the characteristic equation to calculate the roots k_{sn}, but only included the shell force terms in the force expressions (11) to (14). In contrast, the discrete stiffener model excluded the shell stiffener parameters from the equations of motion, but used the full force expressions (11) to (14) including the stiffener force terms. Each of these dynamic stiffness matrices, corresponding to a circumferential mode number n, was calculated over a frequency range from 1 Hz up to 3000 Hz.

For each n, the response $\mathbf{U}_n$ was calculated from Equation (17) for the modal component of a unit axial force or a unit radial force. This meant a force vector $\mathbf{F}_n$ with $L_0 = 1/\pi a$ and $S_0 = 1/\pi a$ respectively, and all other force elements set to zero. These values correspond to forces applied at $\theta = 0$. The modal responses were calculated from $n = 1$ to $n = 20$, the $n = 0$ case resulting in singular matrices as described in the previous section and so not included. In each of the axial and radial cases, the driving point response at $x = 0$ and the response at the other end $x = L$ were considered. From the first of Equations (15), it can be seen that the axial responses U_0 and U_L and the radial responses W_0 and W_L at $\theta = 0$ are simply the sums of their modal components. These summed displacements are presented in the following figures.

Figure 3 shows the axial responses. All 20 modal terms were added progressively and plotted at each step to check convergence. It was found that the driving point responses converged to those shown after about 17 terms, although the last few of those only changed the responses between the resonant peaks. The responses at the other end converged after about 10 terms. The comparison of the two models for the driving point clearly shows that they produce similarly shaped responses, but the peaks are in different positions. Some of

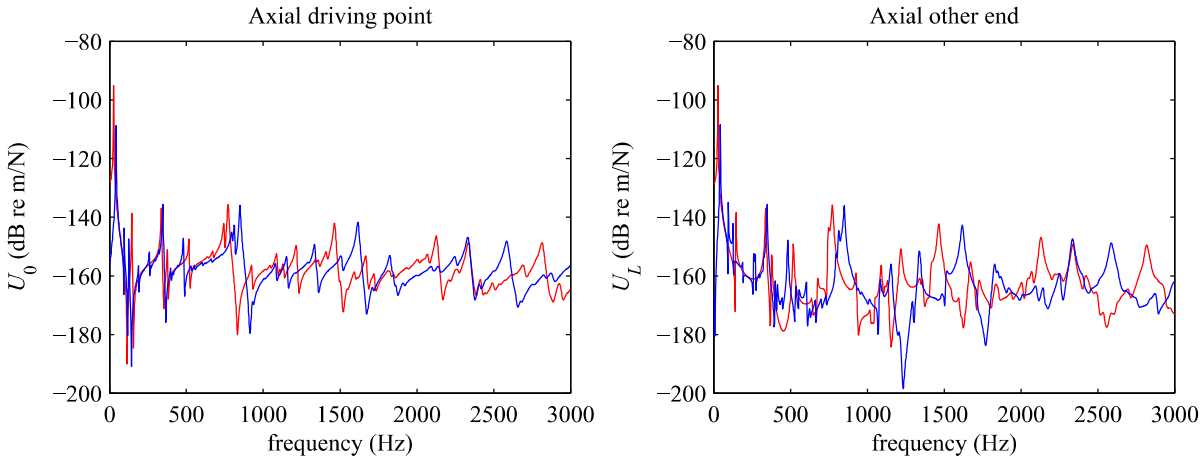

Figure 3 – Axial responses to an axial point load at the driving point and the opposite end of the cylinder. Red is for the shell with smeared stiffeners, blue is for the shell with discrete stiffeners.

the peaks for the smeared stiffener model are higher in frequency than the corresponding ones for the discrete stiffener model, e.g. the resonances at about 500 Hz. However, above 500 Hz many of the smeared shell resonances are lower in frequency by about 10%.. This effect is somewhat less clear in the responses for the opposite end, but still apparent for a number of the peaks. This might be due to differences in the way the extra mass of the ring stiffeners is accounted for. In fact, Equation (5) gives an effective density for the smeared shell of 24% greater than the material density. If the resonance frequencies are inversely proportional to the square root of the mass density, as might be expected from analogy to a simple mass-spring model, then this would lead to a reduction of just over 10% in the frequencies compared to using the unadjusted material density. However, a check using the unadjusted density in place of the effective density did not shift the smeared shell resonances very much and certainly not into alignment with the discrete stiffener model. The description in Leissa (2) is also very clear that the effective mass per unit area should be used in the smeared stiffener model. There is a more complex interplay between the mass and stiffness representations in each of the models.

The levels of the axial responses from the two models are about the same. Adding ring stiffeners should not change the stiffness of the shell in the axial direction much, so smearing out their effects does not change the average stiffness at the driving point for an axial excitation. The discrete stiffener responses do show a number of extra small peaks superimposed on the overall response, particularly noticeable at frequencies below 750 Hz. These could be due to additional modes set up between discrete ring stiffeners encompassing shorter lengths of shell than the total length. These cannot be represented by a smeared shell model.

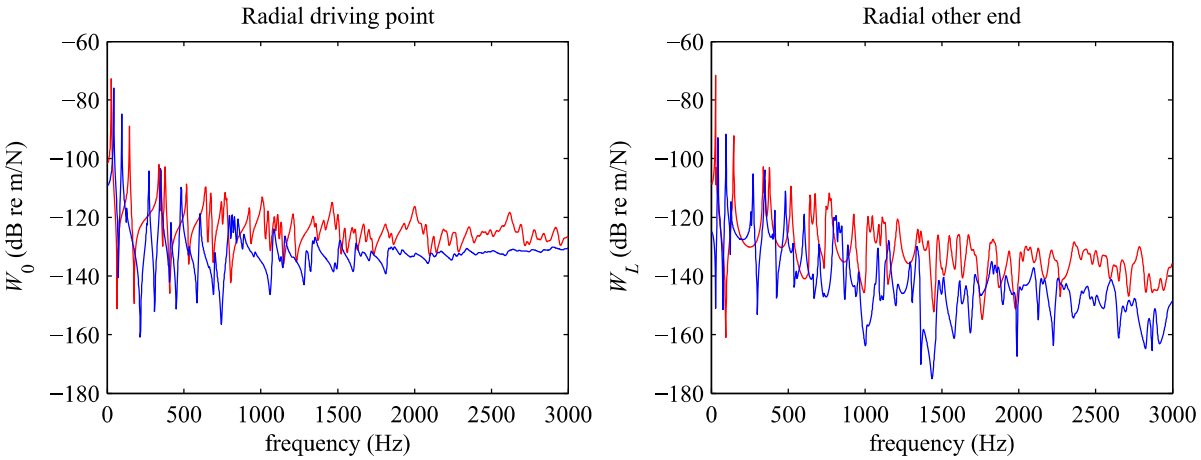

Figure 4 – Radial responses to a radial point load at the driving point and the opposite end of the cylinder. Red is for the shell with smeared stiffeners, blue is for the shell with discrete stiffeners.

The radial responses are shown in Figure 4. Similar numbers of modal terms as for the radial responses were needed for converged results. The same shifting of many of the resonances between models occurs for the radial direction; although it is not clear from the total responses shown, it was in individual modal responses and the summation of the first few terms during convergence checking. However, perhaps most noticeable is that the responses from the smeared shell model are significantly higher in magnitude than those from the discrete stiffener model. In both examples of Figures 3 and 4, the forces are applied at the position of a ring stiffener and the responses are also calculated at the ring stiffeners at each end of the model. The stiffness of the ring comes into play for the radial excitation. The smeared shell model averages this over the whole shell, while the discrete stiffness model represents it directly. Hence the apparent radial stiffness is higher in the discrete stiffener model and the responses are correspondingly lower.

Further work would include investigating the discrepancy between the resonance frequencies shown in the results of each model. This could be through alternative analytical formulations for both smeared and discrete stiffener models, numerical modelling such as the finite-element method, or through experimental measurement of a ring stiffened cylinder. An axisymmetric case should also be developed to calculate the $n = 0$ contributions to the axial and radial displacements u and w and complete the summations that determine the total displacements. Once the modelling is refined, it would be interesting to investigate the effect of stiffeners with random spacing. This could be based on the uniform spacing already considered with say up to ± 20% variation in the axial placement of the stiffeners, while keeping the overall length of the cylindrical shell the same.

4. CONCLUSIONS

Two modelling approaches have been developed to calculate the forced response of a ring stiffened cylindrical shell. One smears the mass and stiffness properties of the ring stiffeners over the whole shell, while the other considers the stiffeners discretely. Each approach uses a similar process to construct a dynamic stiffness matrix for the ring stiffened shell, but accounts for the stiffeners differently. The smeared shell model uses stiffener parameters added into the equations of motion that determine the displacements of the shell, and force terms that only consider the forces arising from the shell. The discrete stiffener model uses the equations of motion for a plain shell, but force terms that include contributions from both the shell and the ring stiffeners.

The calculated results from both models for an example small cylindrical shell showed some differences between the two approaches. The smeared shell model gave many resonance frequencies about 10 % lower than those for the discrete stiffener model. The discrete model showed small additional peaks superimposed on the response between major peaks, probably due to resonances set up between stiffeners at spacings less than the overall length of the cylinder. These cannot be represented by the smeared model. The discrete model also showed lower radial response levels than the smeared model, because the responses were calculated at stiffener positions. The smeared model only averages the stiffener effects over the whole cylinder, while the discrete model applies all the stiffener reaction forces at the stiffener position.

REFERENCES

1. Leissa A. Vibration of Plates. New York: Acoustical Society of America; 1993.
2. Leissa A. Vibration of Shells. New York: Acoustical Society of America; 1993.
3. Ruotolo R. Influence of some thin shell theories on the evaluation of the noise level in stiffened cylinders. Journal of Sound and Vibration. 2002; 255(4):777-88.
4. Gan L, Li X, Zhang Z. Free vibration analysis of ring-stiffened cylindrical shells using wave propagation approach. Journal of Sound and Vibration. 2009; 326(3-5):633-46.
5. Luan Y, Ohrlich M, Jacobsen F. Improvements of the smearing technique for cross-stiffened thin rectangular plates. Journal of Sound and Vibration. 2011; 330(17):4274-86.
6. Junger MC, Feit D. Sound, Structures and Their Interaction. 2nd ed. New York: Acoustical Society of America; 1993.
7. Mace BR. Periodically stiffened fluid-loaded plates, II: response to line and point forces. Journal of Sound and Vibration. 1980; 73(4):487-504.
8. Langley RS. Application of the dynamic stiffness method to the free and forced vibrations of aircraft panels. Journal of Sound and Vibration. 1989; 135(2):319-31.
9. Hodges CH, Power J, Woodhouse J. The low frequency vibration of a ribbed cylinder, part 1: theory. Journal of Sound and Vibration. 1985; 101(2):219-35.
10. Mead DJ, Bardell NS. Free vibration of a thin cylindrical shell with discrete axial stiffeners. Journal of Sound and Vibration. 1986; 111(2):229-50.
11. Mead DJ, Bardell NS. Free vibration of a thin cylindrical shell with periodic circumferential stiffeners. Journal of Sound and Vibration. 1987; 115(3):499-520.
12. Lee J-H, Kim J. Sound transmission through periodically stiffened cylindrical shells. Journal of Sound and Vibration. 2002; 251(3):431-56.
13. Efimtsov BM, Lazarev LA. Forced vibrations of plates and cylindrical shells with regular orthogonal system of stiffeners. Journal of Sound and Vibration. 2009; 327(1-2):41-54.
14. Solaroli G, Gu Z, Baz A, Ruzzene M. Wave propagation in periodic stiffened shells: spectral finite element modeling and experiments. Journal of Vibration and Control. 2003; 9(9):1057-81.
15. Forrest JA. Structural vibration transmission in stiffened structures. Acoustics 2011; 2-4 November 2011; Gold Coast, Australia 2011.
16. Forrest JA. Measured dynamics of a thin cylindrical shell subject to axial excitation. Acoustics 2005; 9-11 November 2005; Busselton, Western Australia 2005. p. 61-6.
17. Forrest JA. Moment control of the sound radiated from an axially excited cylindrical shell. 14th International Congress on Sound and Vibration (ICSV14); 9-12 July 2007; Cairns, Australia 2007.
18. Young WC, Budynas RG. Roark's Formulas for Stress and Strain. 7th ed. New York: McGraw-Hill; 2002.